Through-Bond Indirect and Through-Space Direct Dipolar Coupling ^{31}P MAS NMR Constraints for Spectral Assignment in the Cubic 3 × 3 × 3 Superstructure of TiP_2O_7

Xavier Helluy,[†] Claire Marichal,[‡] and Angelika Sebald*[,§]

Department of Pharmaceutical Sciences, Preformulation/Physical Analysis, Aventis Pharma, Research Center of Vitry-Alfortville, F-94403 Vitry sur Seine Cedex, France, Laboratoire de Matériaux Minéraux, 3 rue Alfred Werner, F-68093 Mulhouse Cedex, France, and Bayerisches Geoinstitut, Universität Bayreuth, D-95440 Bayreuth, Germany

Received: October 12, 1999; In Final Form: January 20, 2000

A ^{31}P solid-state NMR study of TiP_2O_7 is reported. The combined constraints from one-dimensional ^{31}P MAS NMR experiments and from ^{31}P 2D MAS NMR experiments probing through-bond P−O−P connectivities via homonuclear *J* coupling interactions (TOBSY experiments), positively identify the cubic space group $Pa\bar{3}$ with a 3 × 3 × 3 superstructure. Additional ^{31}P 2D MAS NMR experiments, probing spatial connectivities between phosphorus sites via homonuclear dipolar coupling interactions (^{31}P single-quantum−double-quantum correlation MAS NMR experiments), subsequently lead to complete assignment of the 11 distinct crystallographic P sites in the structure of TiP_2O_7 to the corresponding eight resolved resonances in ^{31}P MAS NMR spectra of TiP_2O_7, while ^{31}P RIL ZQT and C7 DQT MAS NMR experiments confirm that TiP_2O_7 and the cubic phase of SiP_2O_7 are isostructural.

Introduction

Subtle aspects of the solid-state structures of crystalline pyrophosphate phases $M^{IV}P_2O_7$ with, e.g., M = Si, Ti, Zr have repeatedly been discussed in relation to the unusual physical properties (e.g., negative thermal expansion coefficients) of these and similar vanadate phases.[1−7] Although phases $M^{IV}P_2O_7$ crystallize in several different structures, the cubic polymorph is based on a particularly simple arrangement of corner-sharing MO_6 octahedra and P_2O_7 groups. In the ideal cubic structure all $P_2O_7^{4-}$ units would have to be present as linear P−O−P moieties for reasons of symmetry. It has been argued that linear P−O−P bonding arrangements in pyrophosphates are energetically less favorable than bent P−O−P arrangements with P−O−P bond angles of ca. 145°.[5] Linear P−O−P pyrophosphate units in $M^{IV}P_2O_7$ phases are partially or completely avoided by distortion of the ideal cubic structure. This distortion, in the form of rotation of the constituent polyhedra, results in a 3 × 3 × 3 superstructure. Although the diffraction evidence for the size of the supercell is unambiguous, the superstructure reflections are generally of low intensity and thus the true structure, including the choice of space group, is less well established. The crystal structure of the cubic phase of SiP_2O_7 with a 3 × 3 × 3 superstructure, based on single-crystal X-ray diffraction data and refinement involving presumed interatomic distances, has been reported[8] in space group $Pa\bar{3}$. An analogous study of TiP_2O_7 based on powder X-ray diffraction data led to an isostructural arrangement.[2] Figure 1 shows a section of the $M^{IV}P_2O_7$ superstructure, illustrating how fairly small rotations from the ideal substructure result in the cubic 3 × 3 × 3 superstructure. The phosphate tetrahedra pairwise share a bridging oxygen atom to form individual $P_2O_7^{4-}$ units. There are six crystallographically distinct $P_2O_7^{4-}$ units in the asymmetric unit. Following Tillmann's numbering scheme for the various crystallographic sites,[8] the pairwise connected phosphorus sites in the structure are P1−O−P8, P2−O−P7, P3−O−P4, P5−O−P6, P9−O−P11, and P10−O−P10. The pyrophosphate units P1−O−P8, P2−O−P7, P3−O−P4, and P5−O−P6 (all these P sites have a relative abundance 3 in the unit cell) feature P−O−P bond angles of ca. 145°. The cubic 3 × 3 × 3 superstructure of space group $Pa\bar{3}$ requires the presence of two further special types of $P_2O_7^{4-}$ units. Both special $P_2O_7^{4-}$ units must reside on proper axes of 3-fold symmetry and thus enforce linear P−O−P arrangements for these two pyrophosphate units, P9−O−P11 and P10−O−P10 (these special three P sites have a relative abundance 1 in the unit cell). In addition to this linearity requirement, the bridging oxygen atom of the P10−O−P10 unit must be located on a center of inversion symmetry.

In the following we will inspect how the three-dimensional arrangement of $P_2O_7^{4-}$ units in the TiP_2O_7 structure is reflected in various one- and two-dimensional ^{31}P MAS NMR experiments. We will explore how experimental ^{31}P MAS NMR evidence may independently discriminate for or against a particular space-group symmetry, and to which extent ^{31}P resonances may unambiguously be assigned to specific P sites in the TiP_2O_7 structure. Our investigation considers ^{31}P MAS NMR constraints derived from through-bond connectivities via homonuclear *J* coupling interactions[9] as well as through-space connectivities revealed by different homonuclear dipolar recoupling experiments.[10,11] We compare the ^{31}P MAS NMR properties of the isostructural phases TiP_2O_7 and SiP_2O_7.

Experimental Section

Compounds. Our samples of TiP_2O_7 and SiP_2O_7 were donated by R. Glaum, Giessen. The purity of the samples was checked by powder X-ray diffraction.

* Corresponding author; angelika.sebald@uni-bayreuth.de.
[†] Aventis Pharma.
[‡] Laboratoire de Matériaux Minéraux.
[§] Universität Bayreuth.

10.1021/jp993626o CCC: $19.00
Published on Web 03/11/2000

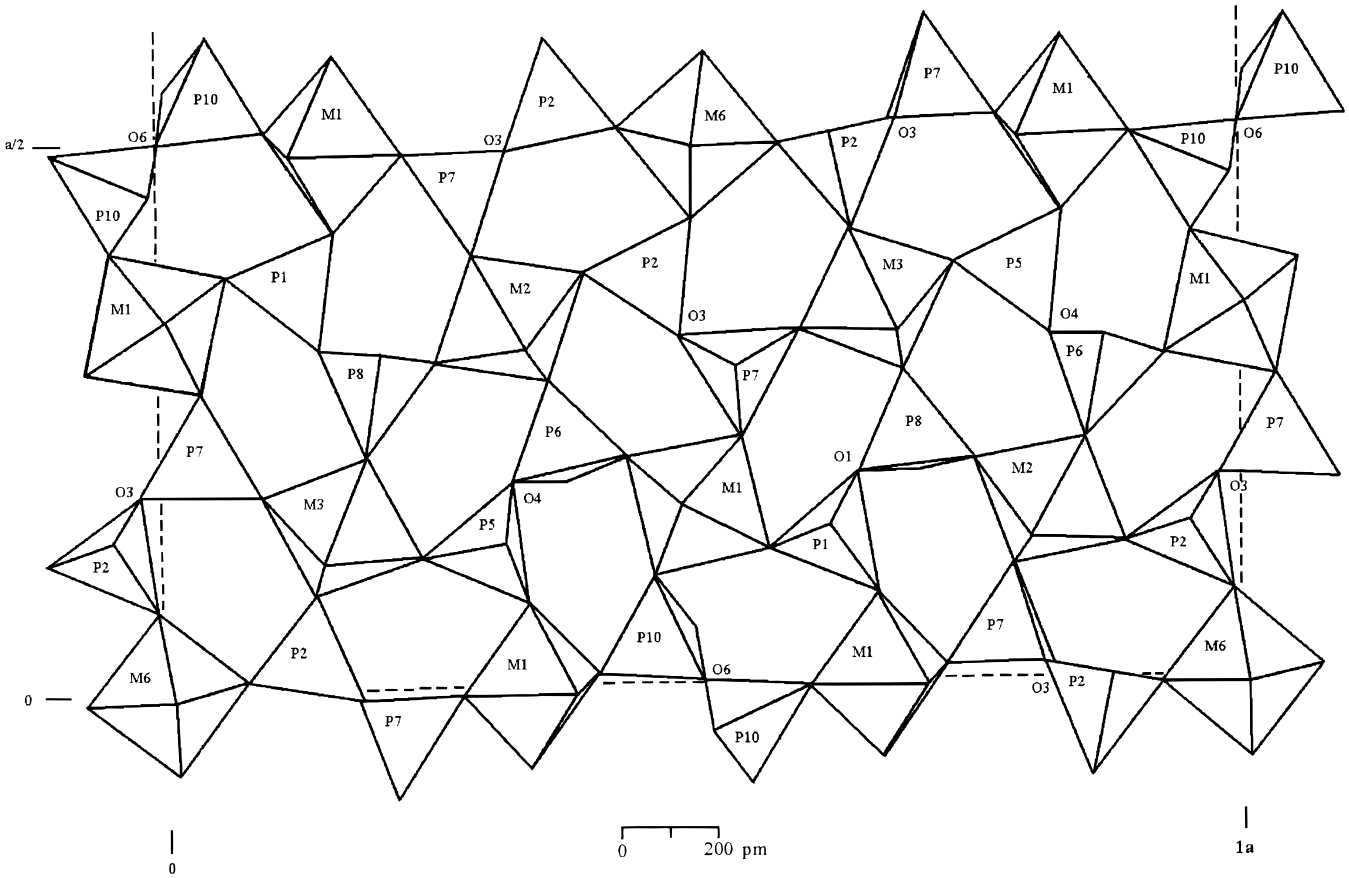

Figure 1. Schematic representation of a partial view of the $M^{IV}P_2O_7$ structure in the cubic $3 \times 3 \times 3$ superstructure of space group $Pa\bar{3}$; adapted from Figure 2 in ref 8.

NMR Experiments. ^{31}P MAS NMR experiments were carried out at room temperature on Bruker MSL 200, MSL 300, DSX 400, and DSX 500 NMR spectrometers, corresponding to ^{31}P Larmor frequencies $\omega_0/2\pi = -81.0$ MHz, $\omega_0/2\pi = -121.5$ MHz, $\omega_0/2\pi = -161.9$ MHz, and $\omega_0/2\pi = -202.5$ MHz, respectively. Standard 4 mm double-bearing Bruker CP MAS probes were used; the samples were contained in 4 mm o.d. ZrO_2 rotors. MAS frequencies in general were in the range $\omega_r/2\pi = 0.8$ kHz to $\omega_r/2\pi = 12$ kHz and were actively controlled to within ± 2 Hz. ^{31}P $\pi/2$ pulse durations were in the range 2.0−4.0 μs. The ^{31}P T_1 relaxation times in TiP_2O_7 and SiP_2O_7 are such that recycle delays of 30−60 s represent the shortest possible limit where no serious distortions of the relative intensities of the various resonances in ^{31}P MAS NMR spectra are observed. Isotropic ^{31}P chemical shielding is quoted with respect to external H_3PO_4 (85 wt % in H_2O), $\omega_{iso}^{CS}(^{31}P) = 0$ ppm. The signs of Larmor frequencies have been defined elsewhere[12] and shielding notation is used.

One- (1D) and two- (2D) dimensional ^{31}P TOBSY [9] (*to*tal through-*b*ond correlation *s*pectroscop*y*) experiments were performed on the MSL 300 spectrometer ($\omega_0/2\pi = -121.5$ MHz, $\omega_r/2\pi = 5.2$ kHz, $\omega^{RF}/2\pi$ 125 kHz, using the condition $k = 8$ cycles per rotation period[9]). 2D ^{31}P TOBSY experiments employed a mixing time of $\tau_m = 19.2$ ms and rotation-synchronized t_1 increments of 192 μs. 1D ^{31}P TOBSY experiments for the determination of $|^2J_{iso}(^{31}P,^{31}P)|$ were recorded for a range of mixing times, incrementing τ_m from $\tau_m = 0$ ms to $\tau_m = 66.5$ ms in steps of 1.9 ms.

A set of 12 ^{31}P 2D zero-quantum transfer (ZQT) RIL[13,14] experiments on TiP_2O_7 was recorded at $\omega_0/2\pi = -121.5$ MHz (MSL 300 spectrometer), with mixing times of 1.1, 2.0, 2.8, 3.6, 5.0, 6.1, 7.5, 8.3, 13.9, 15.0, 20.8, and 24.6 ms. The ^{31}P $\pi/2$ pulse duration for these experiments was 2.0 μs, and the spinning frequency was set to 7.2 kHz; some additional experiments were acquired at $\omega_r/2\pi = 8.1$ kHz. The t_1 increments were equal to one rotation period, 16 transients per increment were accumulated.

^{31}P 2D single-quantum−double-quantum (SQ−DQ) correlation experiments on TiP_2O_7 and SiP_2O_7 were performed at $\omega_0/2\pi = -161.9$ MHz (DSX 400 spectrometer), using the C7[15] pulse sequence for excitation and reconversion of DQ coherences. Excitation and reconversion periods of equal durations (400 μs) were used. With a spinning frequency $\omega_r/2\pi = 10$ kHz, the rf-field strength had to be $\omega^{RF}/2\pi = 70$ kHz in order to fulfill the C7 condition $\omega^{RF} = 7\omega_r$. With these experimental conditions the efficiencies of the C7-DQ excitation amounted to ca. 14% for TiP_2O_7 and SiP_2O_7.

Results and Discussion

^{31}P MAS NMR spectra of TiP_2O_7, obtained at $\omega_0/2\pi = -121.5$ MHz, are shown in Figure 2. Eight resolved ^{31}P resonances A−H with differing widths at half-height (ranging from 36 to 122 Hz) and with different relative intensities can be distinguished. At modest MAS frequencies (e.g., $\omega_r/2\pi = 2.5$ kHz; see Figure 2a) pronounced spinning sideband patterns occur, indicating sizable chemical shielding anisotropies of the various ^{31}P resonances in TiP_2O_7, as is typically found for condensed inorganic phosphates. In addition, shapes and widths of the various ^{31}P resonances depend to different degrees on the MAS frequency (see Figure 2b). Line shape effects of this kind are generally to be expected for extended homonuclear dipolar coupled spin systems (such as the ^{31}P spin systems in $M^{IV}P_2O_7$ phases), where even high MAS frequencies do not

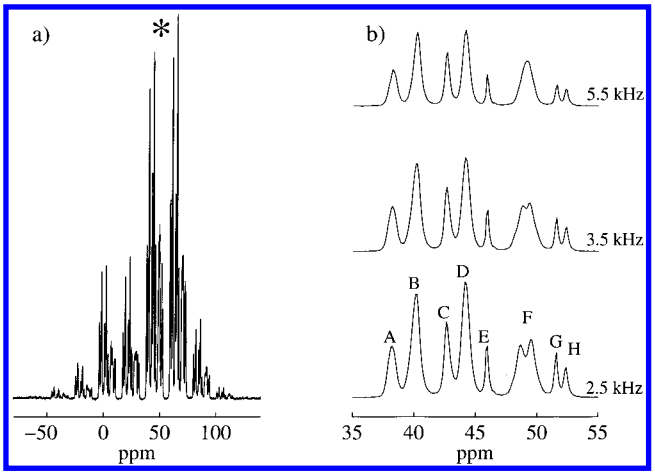

Figure 2. ^{31}P MAS NMR spectra of TiP_2O_7 obtained at a Larmor frequency $\omega_0/2\pi = -121.5$ MHz, with a $\pi/2$ pulse duration of 3.5 μs, $\omega_r/2\pi = 2.5$ kHz, and a recycle delay of 60s: (a) Complete spectral range, * denotes center band region; (b) center band region only, at different MAS frequencies as indicated. Letters A−H (see bottom trace) will be used throughout to refer to the ^{31}P resonances of TiP_2O_7.

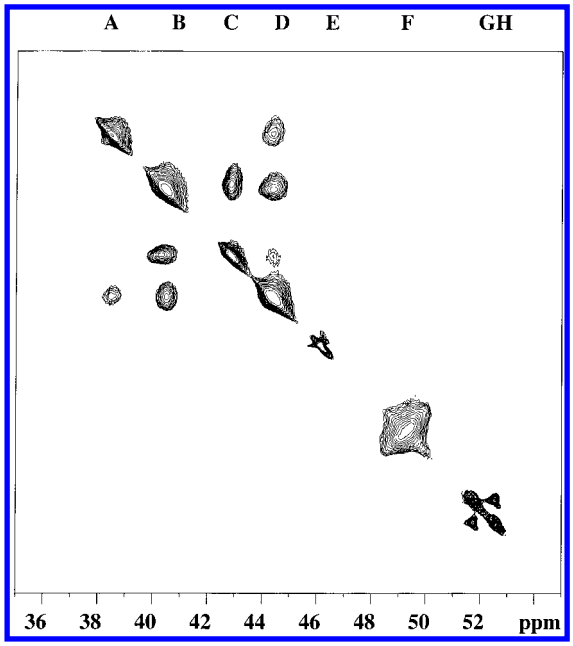

Figure 3. Contour plot of the ^{31}P 2D TOBSY MAS NMR experiment[9] on TiP_2O_7 ($\omega_0/2\pi = -121.5$ MHz, $\omega_r/2\pi = 5.2$ kHz, mixing period 19.2 ms). The diagonal corresponds to the 1D ^{31}P MAS NMR spectrum, the labeling A−H of the ^{31}P resonances is given on the top *y*-axis.

completely average out the effects of homonuclear dipolar coupling interactions.[16] This property of homonuclear dipolar coupled spin systems under MAS conditions considerably complicates the interpretation of MAS NMR spectra of such spin systems by "inspection". Nevertheless, from ^{31}P MAS NMR spectra of TiP_2O_7 at this point we can safely draw the following conclusions regarding the crystallographic space group. An ideal cubic structure, $Pa\bar{3}$, is ruled out, as this would be consistent only with the presence of a single ^{31}P resonance. Similarly, all subgroups with less than nine independent crystallographic P sites per asymmetric unit can be excluded. Allowing for the occurrence of incomplete spectral resolution in the ^{31}P MAS NMR spectra, in principle a large number of crystallographic space groups still remains possible. The remaining possibilities include space group $Pa\bar{3}$ with a cubic $3 \times 3 \times 3$ superstructure (11 independent P sites in the asymmetric unit) and all of its subgroups. These derivatives of the cubic $3 \times 3 \times 3$ superstructure would require between 22 (space group $P2_13$) and 216 (space group $P1$) independent P sites per asymmetric unit. From ^{31}P MAS NMR spectra alone, for the moment we have to leave the choice of space group open. However, we mention that the relative intensities of the resonances ^{31}P(E), ^{31}P(G), and ^{31}P(H) would be consistent with assigning these to phosphorus sites P10 (^{31}P(E)) and to the P9−O−P11 unit (^{31}P(G) and ^{31}P(H), or vice versa) in the cubic $3 \times 3 \times 3$ superstructure of space group $Pa\bar{3}$: according to the requirements of this space group, we would have to observe eight ^{31}P resonances of relative intensity 3 and three ^{31}P resonances of relative intensity 1 for the special P sites P9, P10, and P11. Experimentally, we find integrated intensities of 3.0:6.8:2.9:6.9:1.0:6.0:0.8:0.8 for the eight resolved resonances ^{31}P(A) to ^{31}P(I). Likewise, within experimental error these relative intensities would also be consistent with the requirements of a $3 \times 3 \times 3$ superstructure of space group $P2_13$, which, however, would correspond to a higher degree of spectral overlap in the ^{31}P MAS NMR spectra. Before adopting a final choice of space group, we need additional supporting evidence from further ^{31}P MAS NMR experiments.

In addition to the number of independent P sites (number of ^{31}P resonances), the number of different $P_2O_7^{4-}$ groups characterize and distinguish the particular space groups (e.g., six for the $3 \times 3 \times 3$ superstructure of space group $Pa\bar{3}$, 11 for the $3 \times 3 \times 3$ superstructure of space group $P2_13$). The NMR interaction that permits specific identification of intra-$P_2O_7^{4-}$ P−O−P through-bond connectivities, is the homonuclear *J* coupling interaction $^2J_{iso}(^{31}P,^{31}P)$. The TOBSY[9] pulse sequence is designed for homonuclear *J* polarization transfer under MAS conditions, while suppressing homonuclear dipolar and anisotropic chemical shielding interactions. Since spectral resolution of the respective *J* coupling patterns in 1D MAS NMR spectra is not required for the 2D TOBSY experiment to successfully identify *J* connectivities, a ^{31}P 2D TOBSY experiment on TiP_2O_7 permits us to count the number of crystallographically distinct $P_2O_7^{4-}$ units present. The contour plot of a ^{31}P 2D TOBSY experiment on TiP_2O_7 ($\omega_0/2\pi = -121.5$ MHz, $\omega_r/2\pi = 5.2$ kHz) with a mixing time τ_m 19.2 ms is shown in Figure 3. The ^{31}P resonances (A−H), corresponding to the 1D ^{31}P MAS NMR spectrum (compare Figure 2b) are displayed along the diagonal of the 2D contour plot, the off-diagonal peaks indicate pairwise *J* connectivities. Four connectivities are immediately identified, relating ^{31}P(A)−^{31}P(D), ^{31}P(B)−^{31}P(C), ^{31}P(B)−^{31}P(D), and ^{31}P(G)−^{31}P(H) by mutual *J* coupling. At the MAS frequency chosen for the 2D TOBSY experiment ($\omega_r/2\pi = 5.2$ kHz), resonance ^{31}P(F), which must represent different P sites, is not resolved (compare Figure 2b). However, the contour plot of the 2D TOBSY experiment displays a characteristic broadening of this spectral region around the diagonal and thus suggests ^{31}P(F) as representing a P−O−P pair. The only ^{31}P resonance not revealing any *J* connectivity is ^{31}P(E). All combined evidence from ^{31}P 1D MAS and 2D TOBSY NMR experiments is consistent with the cubic $3 \times 3 \times 3$ superstructure of space group $Pa\bar{3}$ as the correct choice, despite the lack of spectral resolution in the ^{31}P 1D MAS NMR spectra. There have to be six different P−O−P connectivities, four of which the 2D TOBSY experiment positively identifies. The sixth connectivity concerns the special P10−O−P10 pyrophosphate unit. The two P10 sites in this unit are related by inversion symmetry, which renders the corresponding two ^{31}P spins magnetically equivalent and thus prevents positive identification via *J* coupling between them. Accordingly, resonance ^{31}P(E) can now be assigned to site P10. The 2D TOBSY experiment confirms our previous tentative assignment of the pair of resonances ^{31}P(G)−^{31}P(H) as representing the P9−O−P11 unit. It further shows that the

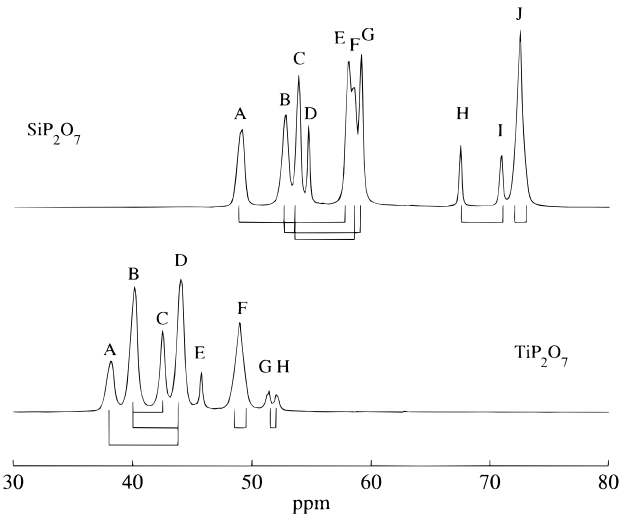

Figure 4. Comparison of 1D ^{31}P MAS NMR spectra of SiP_2O_7 (top trace) and TiP_2O_7 (bottom trace) at a Larmor frequency of $\omega_0/2\pi = -81.0$ MHz and $\omega_r/2\pi = 9.0$ kHz. The pairwise through-bond ^{31}P−O−^{31}P connectivities as determined by ^{31}P 2D TOBSY MAS NMR experiments on TiP_2O_7 (this work) and SiP_2O_7[20,27] are indicated.

most intense resonances, ^{31}P(B), ^{31}P(D), and ^{31}P(F), in the 1D MAS NMR spectra are incompletely resolved and each represent two different P sites in the structure, which then accounts for the required 11 distinct ^{31}P resonances / 11 distinct P sites in the asymmetric unit. With ^{31}P(E) assigned to site P10, we are now left with the task of assigning the remaining 10 P sites to the ^{31}P resonances in TiP_2O_7. No further clues in this regard can be obtained from consideration of the *J* connectivities alone.

Before attempting further assignment, it is instructive to compare the results of ^{31}P 1D MAS and 2D TOBSY NMR experiments on TiP_2O_7 and the cubic phase of SiP_2O_7. This comparison is shown in Figure 4. One may be tempted to expect similar 1D ^{31}P MAS NMR spectra for two isostructural compounds. In fact, the two spectra differ considerably with regard to isotropic ^{31}P chemical shielding range and spread, which obviously are strongly influenced by the nature of the cation M^{4+} (M = Si, Ti). A simple comparison of these two ^{31}P MAS NMR spectra immediately disqualifies qualitative resonance-assignment approaches based on P−O−P bond angles, "local symmetry" arguments, or similar. "Trends" in isotropic ^{31}P chemical shielding in general are *not* a suitable guide for the assignment of resonances in extended inorganic phosphate network structures, as has also been demonstrated for the crystalline ortho-phosphate $Cd_3(PO_4)_2$[17,18] and the layered aluminophosphate Mu-4.[19] The identity of the topologies of the ^{31}P spin networks as well as the analogy between them in TiP_2O_7 and SiP_2O_7 are not primarily encoded in isotropic ^{31}P chemical shielding values but are reflected in parameters such as identical numbers of *J* connectivities, similar magnitudes of values $|^2J_{iso}(^{31}P,^{31}P)|$, relative intensities of resonances as required by the crystallographic space group, similarities of distance connectivities as detected by probing dipolar-coupling connectivities (see below), or relative mutual orientations of ^{31}P chemical shielding tensors.[20] From the oscillatory behavior of the *J* polarization transfer as a function of mixing time in a 1D version of the TOBSY experiment,[9] it is possible to determine $|^2J_{iso}(^{31}P,^{31}P)|$ for those ^{31}P−O−^{31}P pairs with ^{31}P resonances sufficiently well resolved to allow selective inversion of one of the two ^{31}P spins in the pair. For TiP_2O_7 we find $|^2J_{iso}(^{31}P,^{31}P)| = 31 \pm 2$ Hz (^{31}P(A)−^{31}P(D)), 21 ± 2 Hz (^{31}P(B)−^{31}P(C)), 18 ± 2 Hz (^{31}P(G)−^{31}P(H)), similar to the values found for SiP_2O_7[20] and $Cd_2P_2O_7$.[21] The magnitude *and* sign of $^2J_{iso}(^{31}P,^{31}P) = -19.5 \pm 2.5$ Hz have been determined for the pyrophosphate moiety in solid $Na_4P_2O_7 \cdot 10H_2O$.[22] With the negative sign of $^2J_{iso}(^{31}P,^{31}P)$ established, our finding of the smallest value $|^2J_{iso}(^{31}P,^{31}P)|$ for the ^{31}P(G)−^{31}P(H) pair in TiP_2O_7 is consistent with the largest P−O−P bond angle (180°) in the corresponding crystallographic P9−O−P11 unit.

After this excursion, we return to our remaining assignment task for TiP_2O_7. Initially, in the absence of any further constraints, assigning 11 resonances to 11 crystallographic sites would correspond to 11! = 39 916 800 possible assignment permutations. The constraints from the TOBSY experiments drastically reduce the number of possible assignment permutations: with the P10−O−P10 site identified as corresponding to ^{31}P(E), and the P9−O−P11 unit ascribed to the ^{31}P(G)−^{31}P(H) pair, the 'TOBSY pairs' ^{31}P(A)−^{31}P(D), ^{31}P(B)−^{31}P(C), ^{31}P(B)−^{31}P(D), and ^{31}P(F)−^{31}P(F) remain to be matched to the "crystallographic pairs" P1−O−P8, P2−O−P7, P3−O−P4, and P5−P6, and the individual ^{31}P resonances within the pairs need to be matched to the individual P sites. This leaves us with 3072 possible assignment permutations of which only 384 will be experimentally distinguishable owing to the spectral overlap for resonances ^{31}P(B), ^{31}P(D), and ^{31}P(F). To attempt assignment, we now need to probe inter-$P_2O_7^{4-}$ group spatial distance connectivities and, therefore, have to turn to ^{31}P homonuclear dipolar recoupling experiments under MAS conditions. Many different experimental approaches exist,[10,11] and the selection of the most suitable experimental tools and strategies for the analysis of the experimental data critically depends on the properties of the spin system at hand. The nonisolated ^{31}P spin systems in solid pyrophosphates are characterized by relatively large isotropic as well as anisotropic ^{31}P chemical shielding interactions, and by the simultaneous presence of large intra-$P_2O_7^{4-}$ -group ("nearest neighbor") and numerous different inter-$P_2O_7^{4-}$ -group medium ("next-nearest neighbors") to small ("other neighbors") ^{31}P−^{31}P dipolar coupling interactions. Individually distinct medium-range, inter-$P_2O_7^{4-}$ -group relationships exist among the various $P_2O_7^{4-}$ groups in the three-dimensional structure[8] (for illustration see, for instance, Figure 1). For purposes of assigning the ^{31}P resonances to the crystallographic P sites it should be sufficient to identify these next-nearest-neighbor distance connectivities, in addition to the already known pairwise intra-$P_2O_7^{4-}$ -group, nearest-neighbor connectivities. Typical nearest-neighbor, intra-$P_2O_7^{4-}$ -group ^{31}P−^{31}P distances are ca. 300 pm, while next-nearest-neighbor, inter-$P_2O_7^{4-}$ -group ^{31}P−^{31}P distances are in the range 400−500 pm (see Table 1).[8] The properties of the ^{31}P spin system in TiP_2O_7 require good chemical shielding compensation and "broad-banded" performance of the homonuclear dipolar-recoupling schemes to be used. With this selection criterion in mind, we use 2D ^{31}P ZQT RIL[13,14] and SQ−DQ correlation MAS NMR experiments, employing the C7[15] sequence for excitation and reconversion of double-quantum coherences. The application of dipolar recoupling experiments to multispin systems, or rather the interpretation of these experimental data may be plagued by fundamental difficulties arising from the multispin dynamics involved. Reliable "simple" answers of the yes/no type (or, similarly, assignment of individual resonances) may only be expected as long as we can operate in a regime of short mixing times. A regime of relatively short mixing times in this context may be loosely defined as a regime where additional complications arising from, e.g., relaxation effects and/or relayed transfer processes occurring at long(er) mixing times, may be neglected. What precisely may qualify as a "safe" regime strongly depends not only on the given spin system itself

TABLE 1: Distances (pm) between P Sites P1 to P11 in SiP_2O_7 According to Single-Crystal X-ray Diffraction,[8] within a Cutoff Radius of 800 pm

	P1	P2	P3	P4	P5	P6	P7	P8	P9	P10	P11
P1	411	659	429	460	435	478	403	303	633	420	665
	411	677	659	662	455	616	463	477	681	448	768
	700	744	682	690	619	662	692	674			
		778	700		691	672		728			
			726		728	723					
						772					
P2	659	389	430	488	472	396	299	614	700	746	431
	677	389	450	626	663	693	446	626			662
	744	484	657	688	758	693	467	653			
	778	484	748	711	771	694	672	686			
		621					686	761			
P3	429	430	639	304	445	398	437	427	450	695	664
	659	450	639	419	667	464	477	467			749
	682	657	676	654	671	705	705	627			
	700	748	676	701	692	757	711	661			
	726			745	757						
				760							
P4	460	488	304	447	456	422	432	401	424	721	631
	662	626	419	447	636	433	669	480	749		699
	690	688	654		668	631	693	653			
		711	701		672	667	717	719			
			745		726	742		756			
			760		730						
P5	436	472	445	456	644	301	408	415	474	441	448
	455	663	667	636	644	399	626	443		441	
	619	758	671	668	748	655	653	692			
	691	771	692	672	748		724	768			
	728		757	726			761				
				730							
P6	478	397	398	422	301	481	440	445	662	440	691
	616	693	464	433	399	481	617	675	724	707	702
	662	693	705	631	655		687	678			
	672	694	757	667			706	706			
	723			742			748	733			
	772										
P7	402	299	437	432	498	440	686	420	641	607	442
	463	446	477	669	626	617	686	455	724	736	
	692	467	705	693	653	687	695	714			
		672	711	717	724	796	695	761			
		686			761	748					
P8	303	614	427	401	415	445	420	670	427	667	456
	477	626	467	480	443	675	455	670	738	640	
	674	653	627	653	692	678	714	711			
	728	686	661	756	768	706	761	711			
		761				733					
P9	633	450	450	424	474	662	641	427			313
	633	450	450	424	474	662	641	427			
	633	450	450	424	474	662	641	427			
	681	700		749		724	724	738			
	681	700		749		724	724	738			
	681	700		749		724	724	738			
P10	420	746	695	721	441	440	607	667		309	
	420	746	695	721	441	440	607	667			
	420	746	695	721	441	440	607	667			
	448				661	707	736	694			
	448				661	707	736	694			
	448				661	707	736	694			
P11	665	431	664	631	448	691	442	456	313		
	665	431	664	631	448	691	442	456			
	665	431	664	631	448	691	442	456			
	768	662	749	699		702					
	768	662	749	699		702					
	768	662	749	699		702					

but also on the dipolar-recoupling scheme applied. Unfortunately, for multispin systems there are no simple, clear-cut, and reliable criteria defining a "safe" regime. For these reasons we will consider the combined results of two different homonuclear dipolar recoupling strategies: the RIL approach features zero-quantum-transfer characteristics,[13,14] while the C7-based experiment is described by the evolution of a "double-quantum"

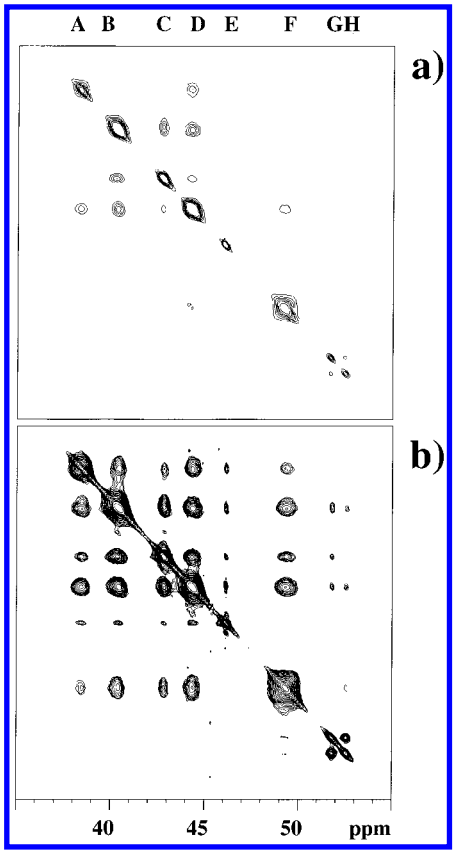

Figure 5. Contour plots of ^{31}P 2D RIL[13,14] ZQT MAS NMR experiments on TiP_2O_7 ($\omega_0/2\pi = -121.5$ MHz, $\omega_r/2\pi = 7.2$ kHz) with mixing times of 7.5 ms (a) and 24.6 ms (b). The ^{31}P resonance positions A−H are indicated on the top *y*-axis.

Hamiltonian.[15] Our guide in approaching final solution(s) for the remaining assignment task will have to be the agreement and the consistency of the results obtained from these two different experimental options. We are now ready to discuss our experimental ^{31}P C7-based SQ−DQ-correlation and RIL ZQT MAS NMR results on TiP_2O_7.

First we inspect how the $^{31}P-^{31}P$ distance connectivities in TiP_2O_7 are reflected in ^{31}P 2D ZQT RIL experiments. A total of 12 experiments with mixing times ranging from $\tau_m = 1.1$ ms to $\tau_m = 24.6$ ms were performed on TiP_2O_7. Contour plots of two ^{31}P 2D ZQT RIL experiments are shown in Figure 5. For short mixing times, the RIL contour plots ($\tau_m = 7.5$ ms, see Figure 5a) mainly show cross-peaks originating from the large intra-$P_2O_7^{4-}$ -group $^{31}P-^{31}P$ dipolar coupling interactions, thus resembling the appearance of the contour plot of the ^{31}P 2D TOBSY experiment (compare Figure 3) and independently confirming the *J* coupling based ^{31}P 2D TOBSY results. For increasingly longer mixing times ($\tau_m = 24.6$ ms; see Figure 5b) additional buildup of cross-peaks due to inter-$P_2O_7^{4-}$ -group $^{31}P-^{31}P$ dipolar coupling interactions occurs. The integrated intensities of all cross-peaks from the complete set of experiments, plotted as a function of mixing times and arranged matrix-like in the order of the resonances ^{31}P(A) to ^{31}P(H), create a 8×8 experimental buildup-curve arrangement, as shown in Figure 6a. On the basis of the known structure of the isostructural SiP_2O_7 phase,[8] it is possible to calculate hypothetical buildup curves between all crystallographic sites P1 to P11 in order to compare them to the experimentally obtained buildup curves as follows.[17] We assume that the RIL ZQT scheme is governed by a "purely dipolar" lowest-order average Hamiltonian, $\bar{H}_D^0$. This type of average Hamiltonian conserves the sum polarization and thus permits describing the transfer dynamics

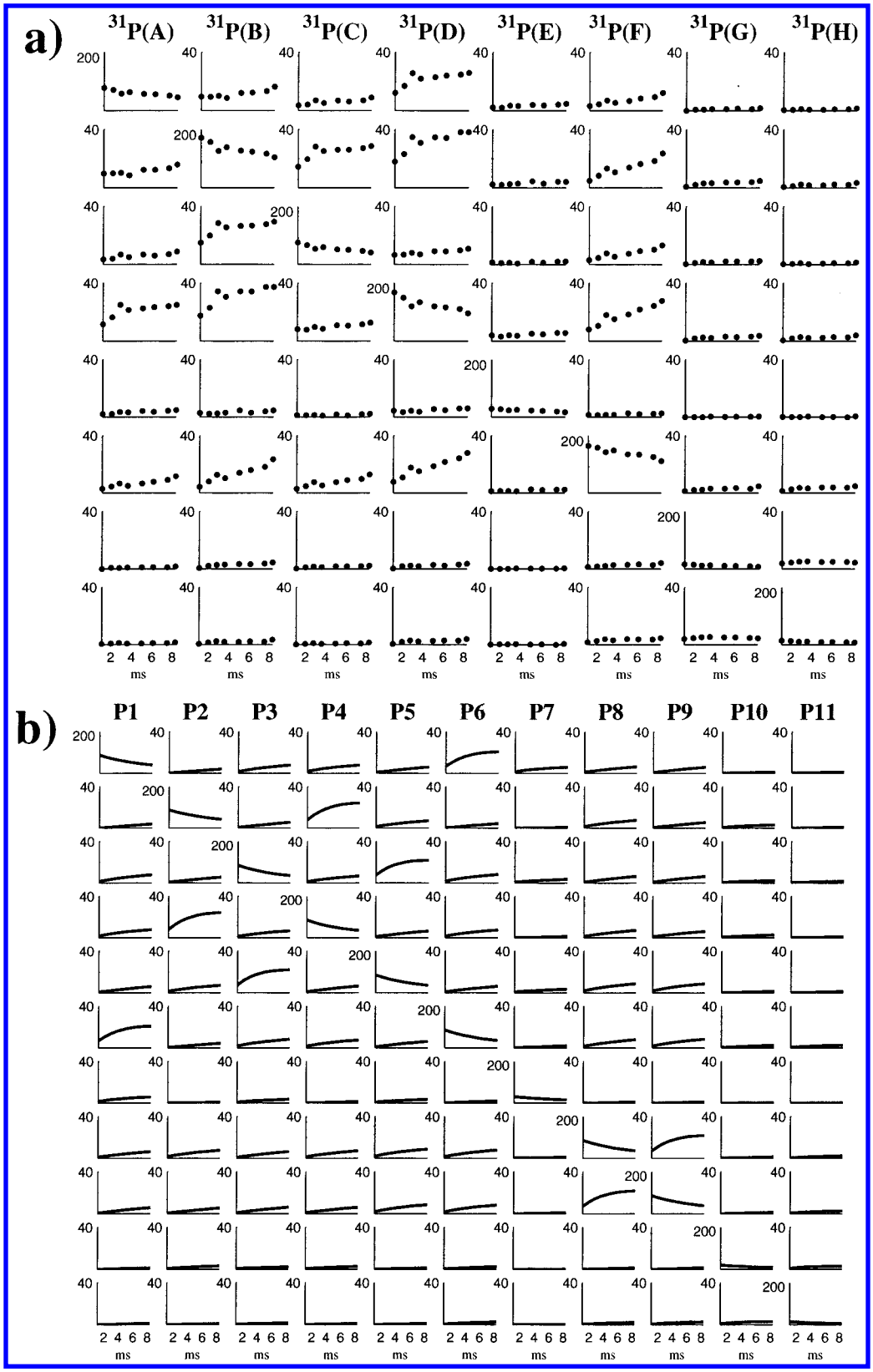

Figure 6. ^{31}P 2D RIL buildup curves with identical scaling of the *y*-axes (au) (200 for diagonal, 40 for off-diagonal elements): (a) experimental ^{31}P NMR data, arranged in the order of ^{31}P resonances A−H; (b) calculated buildup curves (see Tables 1 and 2), arranged in the order of crystallographic sites P1−P11. Note the large differences in relative intensities between individual buildup curves.

by a kinetic exchange matrix **S**,[23] where the matrix elements S_{kl} are proportional to the squared value of the dipolar coupling constant between spins k and l and are related to the corresponding internuclear distance r_{kl} by S_{kl} = constant·r_{kl}^{-6} (see Tables 1 and 2). Arranged in the order P1 to P11, these calculated buildup curves are shown in Figure 6b. Note the large differences in relative intensities between individual buildup curves. To compare experimentally determined and calculated hypothetical buildup curves, the calculated, SiP_2O_7-structure-based 11 × 11 buildup curves have to be condensed into the

TABLE 2: Exchange Matrix *S* (au) As Calculated from the Single-Crystal X-ray Diffraction Data of SiP_2O_7[8] for a Cutoff Radius of 800 pm

	P1	P2	P3	P4	P5	P6	P7	P8	P9	P10	P11
P1		0.33	1.97	1.27	2.92	1.37	3.46	14.04	0.77	9.14	0.49
P2	0.33		2.97	1.08	1.13	2.81	16.59	0.63	0.25	0.17	5.02
P3	1.97	2.97		14.88	1.65	3.65	2.46	2.90	3.61	0.27	0.52
P4	1.27	1.08	14.88		1.61	3.63	1.81	3.47	5.32	0.21	0.73
P5	2.92	1.13	1.65	1.61		15.93	2.59	3.41	2.64	4.44	3.73
P6	1.37	2.81	3.65	3.63	15.93		1.79	1.65	0.56	4.40	0.52
P7	3.46	16.59	2.46	1.81	2.59	1.79		3.08	0.64	0.79	4.01
P8	14.04	0.63	2.90	3.47	3.41	1.65	3.08		5.16	0.61	3.35
P9	0.26	0.09	1.20	1.77	0.88	0.19	0.21	1.72			10.56
P10	3.05	0.06	0.09	0.07	1.48	1.47	0.26	0.20			
P11	0.16	1.67	0.17	0.24	1.24	0.18	1.34	1.12	10.56		

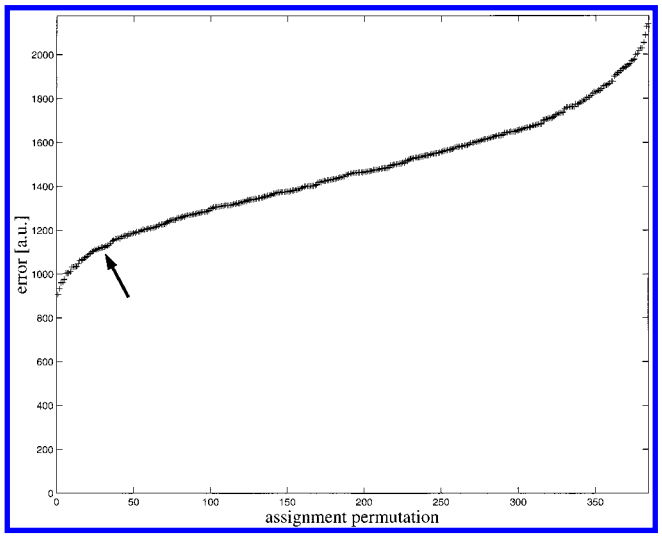

Figure 7. Assignment permutations plotted as a function of the overall root-mean-square error between calculated and experimental buildup curves. For the error calculation only the off-diagonal buildup curves are taken into account. The arrow indicates the assignment permutation (29th) in agreement with the ^{31}P 2D SQ−DQ correlation MAS NMR experiment on TiP_2O_7 (see Figures 8 and 9 and text further below).

spectrally resolved 8 × 8 experimental buildup-curve arrangement. For all the assignment permutations compatible with the TOBSY constraints, the sets of calculated and experimental buildup curves are then compared to each other, and all assignment permutations are subsequently listed according to the total root-mean-square errors between experimental and calculated buildup curves. Figure 7 illustrates the range of relative error for the set of 384 distinguishable (due to spectral overlap) assignment permutations compatible with the TOBSY constraints. The plot in Figure 7 suggests that quite a number of permutations may be excluded but does not provide a well-defined best solution.

Despite the availability of the TOBSY constraints, the ^{31}P spin system in TiP_2O_7 qualifies as a tough case regarding spectral assignment based on ^{31}P RIL ZQT buildup curves, mainly for two reasons. First, the RIL ZQT experiments on TiP_2O_7 are afflicted by the lack of spectral resolution, which considerably reduces the amount of diagnostically useful information. The second difficulty arises from the large differences in relative intensities between several of the buildup curves, as well as from the low relative intensities of some of the diagnostically most important buildup curves concerning sites/resonances with good spectral resolution. The resulting dilemma is further illustrated in Figure 8: in a zoom version the experimental NMR data points are shown in comparison to the calculated buildup curves for the assignment permutation with the lowest overall error and for the 29th-best permutation (see arrow in Figure 7). For instance, the 29th-best assignment permutation yields better agreement between experimental and calculated buildup curves for a larger number of curves, but predominantly for buildup curves with low relative intensities. However, the experimental buildup curves altogether reproduce well the calculated SiP_2O_7-structure-based buildup curves. In this way, the RIL ZQT experiments independently confirm that the cubic phase of SiP_2O_7 and TiP_2O_7 indeed are isostructural. Possible *minor* differences in internuclear P−P distances between these two structures could not satisfactorily account for the inability to discriminate between alternative assignment permutations in this case. Furthermore, the procedure chosen to match experimental and calculated RIL buildup curves (as described elsewhere in detail[17]) involves several further underlying assumptions. It neglects relaxation effects, isotropic homonuclear *J* coupling, and isotropic and anisotropic chemical shielding interactions. This simplified description of the RIL ZQT experiment has previously been verified to yield excellent agreement between calculated and experimental buildup curves for the ^{31}P spin system in the three-dimensional structure of $Cd_3(PO_4)_2$.[17] However, the ^{31}P spin system in $Cd_3(PO_4)_2$ is characterized by rather evenly distributed next-nearest-neighbor ^{31}P−^{31}P distance connectivities and by small isotropic and anisotropic ^{31}P chemical shielding interactions. The ^{31}P spin system in TiP_2O_7 (with larger isotropic and anisotropic ^{31}P chemical shielding interactions and a far more uneven ^{31}P−^{31}P distance-connectivity distribution) is bound to be a more challenging case for this approach. Rather than pushing the assignment issue based on the ^{31}P RIL ZQT buildup curves any further at this point, we will now inspect how the assignment issue appears in the light of a different ^{31}P homonuclear dipolar-recoupling method.

Several applications of homonuclear SQ−DQ correlation MAS NMR experiments with the C7 sequence[15] as the basic building block for excitation and reconversion of DQ coherences have been reported, ranging from identification of different polymorphs in a $Mg_2P_2O_7$ sample,[24] characterization of the structural organization during the crystallization of vitreous $Li_4P_2S_7$,[25] to the spectral assignment of ^{31}P resonances to crystallographic P sites in $Cd_3(PO_4)_2$[18] and ^{13}C resonances in fully ^{13}C-enriched organic compounds.[26] All these applications have in common the use of short DQ excitation periods and take advantage of another useful feature of SQ−DQ correlation MAS NMR experiments: along the diagonal of the 2D contour plot so-called self-connectivities are displayed, i.e., SQ−DQ correlation MAS NMR experiments also reveal spatial proximity between crystallographically equivalent sites. C7-based ^{31}P SQ−DQ correlation MAS NMR experiments on TiP_2O_7 with a very short DQ excitation period (200 μs; data not shown) essentially reproduce the information obtained from the 2D TOBSY experiment and only show correlations between ^{31}P spins in very close spatial proximity with each other, i.e., intra-$P_2O_7^{4-}$-group connectivies. For slightly longer DQ excitation/reconversion periods (400 μs; see Figure 9) not only all of these correlations are present, but also additional correlation peaks of different intensities appear. In the limit of short DQ excitation periods, Table 1 provides the recipe to assign the ^{31}P resonances according to the observed correlations in the ^{31}P 2D SQ−DQ-correlation MAS NMR experiment. The procedure starts at the known assignment ^{31}P(E) = P10. Apart from the intra-$P_2O_7^{4-}$-group P10−O−P10/^{31}P(E)−^{31}P(E) self-connectivity, site P10 has short next-nearest-neighbor distances to sites P1, P5, and P6 (see also Figure 1). Resonance ^{31}P(E) has three "non-self-

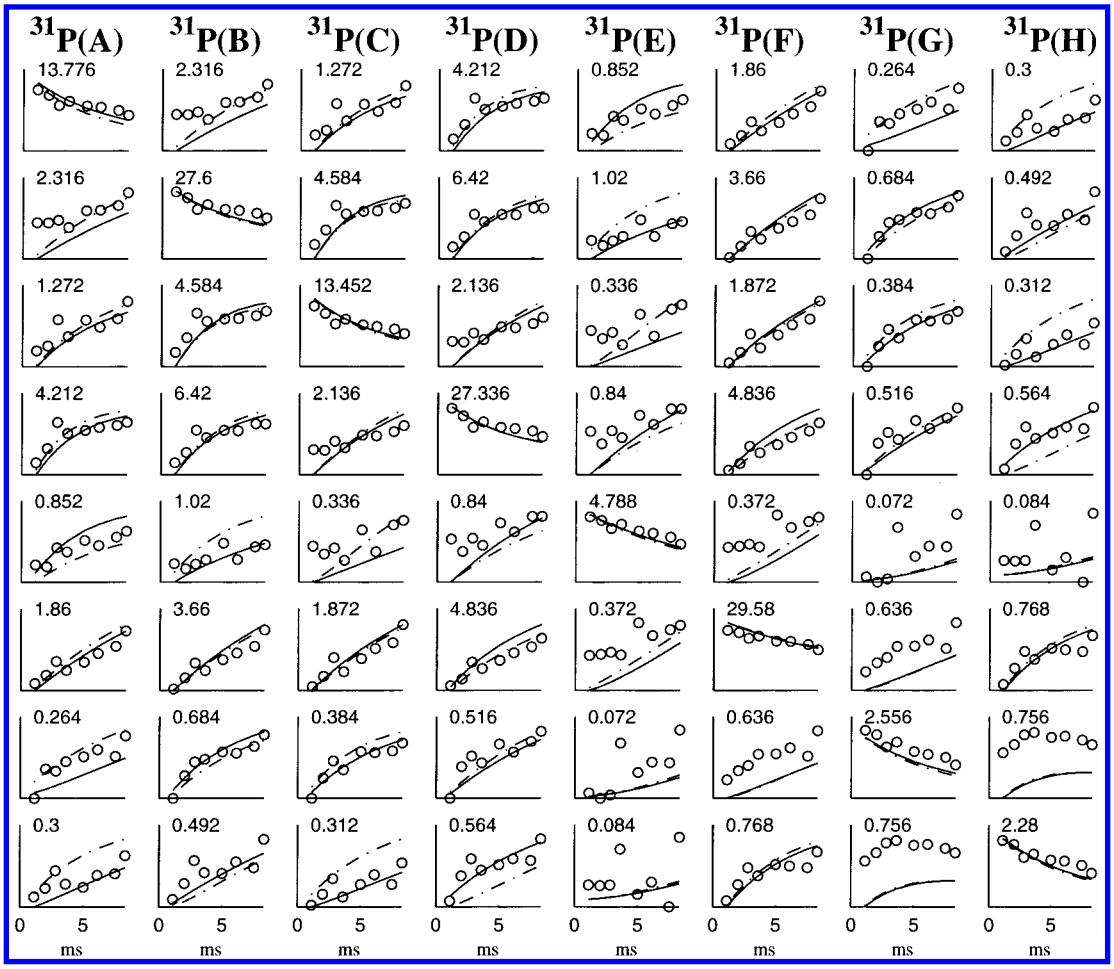

Figure 8. Comparison of experimental (○) to calculated buildup curves for two assignment permutations (solid and dashed lines). For ease of comparison the *y*-axes of all elements are individually scaled as indicated. The dashed lines represent the permutation with the lowest total error: ^{31}P(A), P5; ^{31}P(B), P1,P4; ^{31}P(C), P8; ^{31}P(D), P3,P6; ^{31}P(E), P10; ^{31}P(F), P2,P7; ^{31}P(G), P9; ^{31}P(H), P11. The solid line corresponds to the 29th-best assignment permutation (see Figure 7) and is the assignment permutation in agreement with the ^{31}P 2D SQ−DQ correlation MAS NMR experiment on TiP_2O_7 (see Figure 9 and text further below).

connectivities" (off diagonal) with ^{31}P(A), ^{31}P(B), and ^{31}P(D), relating this set of three resonances to the set of three sites P1, P5, and P6. Among these, the strongest correlation with ^{31}P(E) should be observed for the ^{31}P resonance representing site P1; this is observed for ^{31}P(A) and is also consistent with the "self-connectivity" observed for ^{31}P(A). Identifying ^{31}P(A) = P1 automatically (TOBSY constraint) assigns ^{31}P(D) = P8 and identifies the P5−O−P6 unit with the ^{31}P(B)−^{31}P(D) "TOBSY pair". The most intense self-connectivity correlation should be observed for the ^{31}P resonance of site P2, this is the case for ^{31}P(B). With ^{31}P(B) = P2, ^{31}P(C) = P7 completes the ^{31}P(B)-^{31}P(C) "TOBSY pair" assignment of the P2−O−P7 unit. We know that ^{31}P(G)−^{31}P(H) must represent the P9−O−P11 unit, and thus, by exclusion, the unresolved resonance ^{31}P(F) must represent the P3−O−P4 unit. The complementary connectivities experienced by sites P9 and P11 finally permit the assignment ^{31}P(G) = P11 and ^{31}P(H) = P9, and also ^{31}P(B) = P5 and ^{31}P(D) = P6. It may be easily verified by trial and error that the assignment permutation

^{31}P resonance	A	B	C	D	E	F	G	H
P site	1	2, 5	7	6, 8	10	3, 4	11	9

is the only one not leading to contradictions in the connectivity correlations in the ^{31}P 2D SQ−DQ correlation MAS NMR experiment on TiP_2O_7, as depicted in Figure 9. This assignment permutation is the 29th-best of 384 permutations from consideration of the overall error of the RIL buildup curves (see Figures 7 and 8).

With regard to spectral assignment, the ^{31}P 2D SQ−DQ correlation MAS NMR experiment on TiP_2O_7 is clearly less hampered by the lack of spectral resolution and the relatively low intensity of resonances ^{31}P(E), ^{31}P(G), and ^{31}P(H) than the RIL ZQT experiment. Hence, the SQ−DQ correlation MAS NMR experiment provides us with a unique assignment permutation. The "goodness" of this solution, however, rests on the validity of the assumption of having employed sufficiently short DQ excitation/reconversion periods in this particular experiment. In this regard, it is reassuring that the assignment permutation from the SQ−DQ correlation MAS NMR experiment on TiP_2O_7 is also present among the lowest total error assignment permutations derived from the RIL ZQT buildup curves alone. The situation for the ^{31}P spin system in SiP_2O_7 is instructive to compare to the TiP_2O_7 case. Again, ^{31}P 2D SQ−DQ correlation MAS NMR experiments on SiP_2O_7 (see Figure 10) provide the following unique assignment permutation.

^{31}P resonance	A	B	C	D	E	F	G	H	I	J
P site	1	2	5	10	8	6	7	11	9	3, 4

In constrast to the TiP_2O_7 case, however, this SQ−DQ-correlation-based assignment permutation for SiP_2O_7 is also the assignment permutation with the lowest overall error obtained from ^{31}P RIL buildup curves.[27] The slightly better resolution in

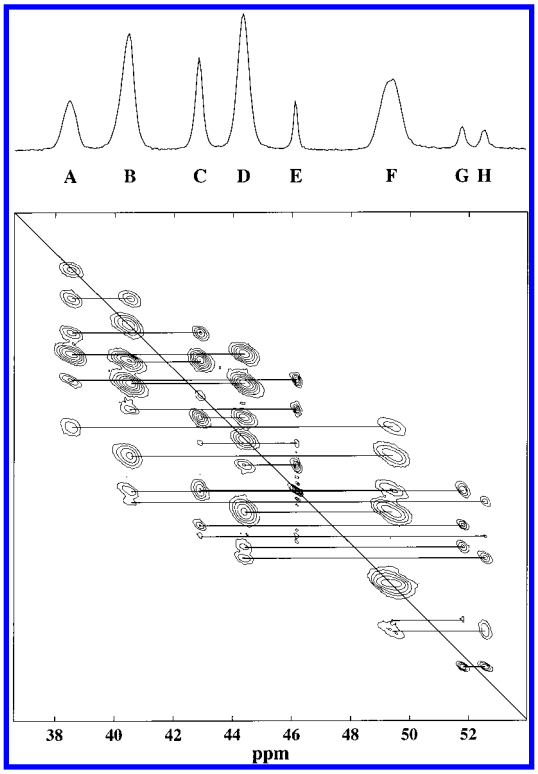

Figure 9. Contour plot of the ^{31}P 2D SQ−DQ correlation MAS NMR experiment[18] on TiP_2O_7, using the C7 sequence[15] as the basic building block for excitation and reconversion of DQ coherences. Experimental conditions: $\omega_0/2\pi = -161.9$ MHz, $\omega_r/2\pi = 10.0$ kHz, excitation and reconversion periods of 400 μs duration each. The corresponding 1D ^{31}P MAS NMR spectrum is shown in the top trace, "self-connectivities" along the diagonal as well as "non-self-connectivities" are marked by lines.

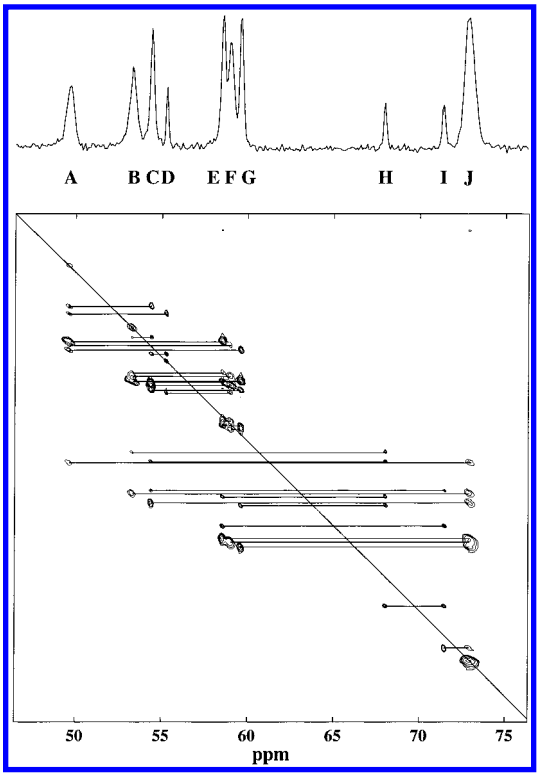

Figure 10. Contour plot of the ^{31}P 2D SQ−DQ correlation MAS NMR experiment[18] on SiP_2O_7, using the C7 sequence[15] as the basic building block for excitation and reconversion of DQ coherences. Experimental conditions: $\omega_0/2\pi = -161.9$ MHz, $\omega_r/2\pi = 10.0$ kHz, excitation and reconversion periods of 400 μs duration each. The corresponding 1D ^{31}P MAS NMR spectrum is shown in the top trace, "self-connectivities" along the diagonal as well as "non-self-connectivities" are marked by lines.

^{31}P MAS NMR spectra of SiP_2O_7 is sufficient to lift the RIL-based assignment ambiguities found for TiP_2O_7. The assignment permutations for SiP_2O_7 and TiP_2O_7 are very closely related. For instance, in both phases the P3−O−P4 units give rise to a poorly resolved ^{31}P resonance with a strongly MAS frequency-dependent line shape (^{31}P(J) in SiP_2O_7 and ^{31}P(F) in TiP_2O_7). For the P9−O−P11 units in both phases it is the less shielded of the two corresponding ^{31}P resonances that represents the P11 site. While P sites P2,P5 and P6,P8 in TiP_2O_7 (^{31}P(B) and ^{31}P(D)) lead to ^{31}P spectral overlap, the corresponding ^{31}P resonances in SiP_2O_7 are resolved (^{31}P(B),^{31}P(C) and ^{31}P(E),^{31}P(F), respectively) but have similar resonance frequencies. Note that the close relationships between SiP_2O_7 and TiP_2O_7 expressed in these assignment permutations are *not* directly reflected in isotropic ^{31}P chemical shielding values. In the absence of the TOBSY constraints, however, ^{31}P 2D RIL ZQT *and* SQ−DQ correlation MAS NMR experiments on TiP_2O_7 *and* SiP_2O_7 would have been faced with unsolvable assignment tasks.

Conclusions

The comparison of the ^{31}P spin systems of the isotructural phases TiP_2O_7 and SiP_2O_7 demonstrates that it may only take minor changes of the properties of the spin system to shift or even possibly interchange the roles of the RIL ZQT and SQ−DQ correlation MAS NMR experiments: with less spectral overlap, less fortuitously diagnostic "self-connectivities", and slightly differently arranged three-dimensional distance connectivities, it is conceivable that there might be cases where the RIL ZQT approach can provide unique assignment while SQ−DQ correlation MAS NMR experiments may be plagued by remaining ambiguities. With regard to the ease of spectral assignment, in most cases SQ−DQ correlation MAS NMR experiments may be the preferable choice, also owing to the convenient feature of having "self-connectivities" as an additional source of information. Our ^{31}P MAS NMR results on TiP_2O_7 and SiP_2O_7 suggest a general protocol, starting from *J* coupling constraints (where applicable), then taking advantage of SQ−DQ correlation MAS NMR experiments for purposes of spectral assignment, and (once the spectral assignment is known) turning to RIL ZQT MAS NMR experiments for further refinement of structural data, such as reconstruction of (parts of) the three-dimensional spin-system topology from additional RIL buildup-curve distance constraints.

Acknowledgment. Support of this work by the Deutsche Forschungsgemeinschaft, the Alexander von Humboldt Foundation, and the Fonds der Chemischen Industrie is gratefully acknowledged. Some solid-state NMR experiments and calculations were performed at the Bayerisches Geoinstitut under the EU "TMR−Large Scale Facilities" program (Contract No. ERBFMGECT980111 to D. C. Rubie). We thank R. Glaum, Giessen, for his generous donation of the TiP_2O_7 and SiP_2O_7 samples, R. Miletich, Zürich, for powder X-ray diffraction measurements, and S. Steuernagel, Bruker Analytik GmbH, Rheinstetten, for running ^{31}P MAS NMR spectra on the DSX 500 spectrometer. The experimental ^{31}P 2D RIL ZQT NMR data on TiP_2O_7 were recorded by J. Kümmerlen. Scientific discussions with S. Dusold, Bayreuth, W. A. Dollase, Los Angeles, and M. Ziliox, Bruker Billerica, are much appreciated.

References and Notes

(1) Khosrovani, N.; Korthuis, V.; Sleight, A. W.; Vogt, T. *Inorg. Chem.* **1996**, *35*, 485.

(2) Sanz, J.; Iglesias, J. E.; Soria, J.; Losilla, E. R.; Aranda, M. A. G.; Bruque, S. *Chem. Mater*. **1997**, *9*, 996.

(3) Korthuis, V.; Khosrovani, N.; Sleight, A. W.; Roberts, N.; Dupree, R.; Warren, W. W., Jr. *Chem. Mater*. **1995**, *7*, 412.

(4) Hudalla, C.; Eckert, H.; Dupree, R. *J. Phys. Chem*. **1996**, *100*, 15986.

(5) Cruickshank, D. W. J. *J. Am. Chem. Soc*. **1961**, *83*, 5486.

(6) Liebau, F. *Structural Chemistry of Silicates*; Springer-Verlag: Berlin, 1985; pp 90−93.

(7) Evans, J. S. O. *J. Chem. Soc., Dalton Trans*. **1999**, 3317.

(8) Tillmanns, E.; Gebert, W.; Baur, W. H. *J. Solid State Chem*. **1973**, *7*, 69.

(9) Baldus, M.; Meier, B. H. *J. Magn. Reson. A* **1996**, *121*, 65.

(10) Bennett, A. E.; Griffin, R. G.; Vega, S. *Recoupling of Homo- and Heteronuclear Dipolar Interactions in Rotating Solids*; NMR Basic Principles and Progress; Springer-Verlag: Berlin Heidelberg, 1994; Vol. 33, pp 3−77.

(11) Dusold, S.; Sebald, A. *Dipolar Recoupling under Magic-Angle-Spinning Conditions*; Annual Reports on NMR Spectroscopy; Academic Press: London, 2000; Vol. 41, pp 185−264.

(12) Levitt, M. H. *J. Magn. Reson*. **1997**, *126*, 164.

(13) Baldus, M.; Tomaselli, M.; Meier, B. H.; Ernst, R. R. *Chem. Phys. Lett*. **1994**, *230*, 329.

(14) Baldus, M.; Meier, B. H. *J. Magn. Reson*. **1997**, *128*, 172.

(15) Lee, Y. K.; Kurur, N. D.; Helmle, M.; Johannesen, O. G.; Nielsen, N. C.; Levitt, M. H. *Chem. Phys. Lett*. **1995**, *242*, 304.

(16) Maricq, M. M.; Waugh, J. S. *J. Chem. Phys*. **1979**, *70*, 3300.

(17) Dusold, S.; Kümmerlen, J.; Schaller, T.; Sebald, A. Dollase, W. A. *J. Phys. Chem. B* **1997**, *101*, 6359.

(18) Dollase, W. A.; Feike, M.; Förster, H.; Schaller, T.; Schnell, I.; Sebald, A.; Steuernagel, S. *J. Am. Chem. Soc*. **1997**, *119*, 3807.

(19) Marichal, C.; Vidal, L.; Delmotte, L.; Patarin, J. *Micropor. Mesopor. Mater*. **2000**, *34*, 149.

(20) Iuliucci, R. J.; Meier, B. H. *J. Am. Chem. Soc*. **1998**, *120*, 9059.

(21) Dusold, S.; Kümmerlen, J.; Sebald, A. *J. Phys. Chem. A* **1997**, *101*, 5895.

(22) Dusold, S.; Milius, W.; Sebald, A. *J. Magn. Reson*. **1998**, *135*, 500.

(23) Ernst, R. R.; Bodenhausen, G.; Wokaun, A. *Principles of Nuclear Magnetic Resonance in One and Two Dimensions*; Clarendon Press: Oxford, U.K., 1987.

(24) Geen, H.; Gottwald, J.; Graf, R.; Schnell, I.; Spiess, H. W.; Titman, J. J. *J. Magn. Reson*. **1997**, *125*, 224.

(25) Schmedt auf der Günne, J.; Eckert, H. *Chem. Eur. J*. **1998**, *4*, 1762.

(26) Hong, M. *J. Magn. Reson*. **1999**, *136*, 86.

(27) Iuliucci, R. J.; Kümmerlen, J.; Meier, B. H.; Sebald, A. Unpublished results.